

OneGAN: Simultaneous Unsupervised Learning of Conditional Image Generation, Foreground Segmentation, and Fine-Grained Clustering

Yaniv Benny
Tel Aviv University
yanivbenny@mail.tau.ac.il

Lior Wolf
Facebook AI Research and Tel Aviv University
wolf@cs.tau.ac.il

Abstract

We present a method for simultaneously learning, in an unsupervised manner, (i) a conditional image generator; (ii) foreground extraction and segmentation, (iii) clustering into a two-level class hierarchy, and (iv) object removal and background completion, all done without any use of annotation. The method combines a generative adversarial network and a variational autoencoder, with multiple encoders, generators and discriminators, and benefits from solving all tasks at once. The input to the training scheme is a varied collection of unlabeled images from the same domain, as well as a set of background images without a foreground object. In addition, the image generator can mix the background from one image, with a foreground that is conditioned either on that of a second image or on the index of a desired cluster. The method obtains state of the art results in comparison to the literature methods, when compared to the current state of the art in each of the tasks.

1. Introduction

We hypothesize that solving multiple unsupervised tasks together, enables one to improve on the performance of the best methods that solve each individually. The underlying motivation is that in unsupervised learning, the structure of the data is a key source of knowledge and each task exposes a different aspect of it. We advocate for solving the various tasks in phases, where easier tasks are addressed first, and the other tasks are introduced gradually, while constantly updating the solutions of the previous sets of tasks.

The method consists of multiple networks that are trained end-to-end and side-by-side to solve multiple tasks. The method starts from learning background image synthesis and image generation of objects from a particular domain. It then advances to more complex tasks, such as clustering, semantic segmentation and object removal. Finally, we show the model’s ability to perform image to image translation. The entire learning process is unsupervised,

meaning that no annotated information is used. In particular, the method does not employ class labels, segmentation masks, bounding boxes, etc. However, it does require a separate set of clean background images, which are easy to obtain in many cases.

Contributions Beyond the conceptual novelty of a method that treats single-handedly multiple unsupervised tasks, which were previously solved by individual methods, the method displays a host of technical novelties, including: (i) a novel architecture that supports multiple paths addressing multiple tasks, (ii) employing bypass paths that allow a smooth transition between autoencoding and generation based on a random seed, (iii) employing a multiplicity of discriminators, each dedicated to a specific path, (iv) the alternating paths, which backpropagate three tasks in each batch, (v) the dual mixup, which employs two random numbers in order to interpolate between latent representations at one hand and between reconstructed and generated images on the other, (vi) an adversarial perceptual loss, (vii) GLU layer-normalization (appendix), and more. Due to each of these novelties, as demonstrated in the ablation studies, we obtain state of the art results compared to the literature methods in each of the individual tasks.

2. Related work

Since our work touches on many tasks, we focus the literature review on general concepts and on the most relevant work. **Generative models** are typically based on Generative Adversarial Networks[9] or Variational Auto-Encoders[16]. In addition, these two can be combined [18]. **Conditional image generation** In conditional image generation, the generated image is conditioned on an initial variable, most commonly, the target class. CGAN[20] and InfoGAN[5] proposed different methods to apply the condition on the discriminator. Our work is more similar to InfoGAN, since we do not use labeled data and the label is not linked to any real image and no conditional discriminator can be applied. The condition is maintained by a classifier that tries to predict the conditioned label

and, as a result, forces the generator to condition the result on that label. **Semantic segmentation** In semantic segmentation, the task is to classify the image pixels based on their class labels. For the supervised setting Unet[21], DeepLab[2], DeepLabV3[3], HRNet[26] have shown great performance leaps using a regression loss. For the unsupervised case, more creative solutions are considered. In [4, 13, 28, 27, 6, 24, 11] a variety of methods have been used including inpainting, learning feature representation, clustering or video frames comparison. In **Clustering**, deep learning methods are the current state of the art. JULE [29] and DEPICT [8], cluster based on a learned feature representation. IIC [11] trains a classifier directly.

The most similar approach to ours is **FineGAN** [23], which our generators and discriminators are based upon. However, there are many significant differences and additions: (i) We added a set of encoders which are trained to support new tasks. (ii) While FineGAN employs one-hot input, our generators use coded input, which is important for our autoencoding path. (iii) We added a skip connection, followed by a mixup module that combines the bypass tensor with the pre-image tensor. The mixup also allows passing only one of the tensors, making either the bypass or the pre-image optional in each flow. (iv) We employ single foreground representation instead of FineGAN’s double hierarchical representation. (v) Our model uses layer normalization [1] instead of batch normalization, which better performs for large number of classes, small batch size, and alternating paths. (vi) We define a new normalization method for the generators, where GLU [7] activation layers were used as non-linear activations. (vii) We add many losses, regularization terms, and training techniques that were not used in FineGAN, many of which are completely novel, as far as we can ascertain. As a result, our work outperforms FineGAN in all tasks and is capable of performing new tasks that its predecessor could not handle.

Mixup [30] is a technique for applying a weighted sum between two or more latent variables in order to synthesize a new latent variable. We use it to mix latent variables that are part encoded by the encoder and part extracted from the one-hot priors. As far as we can ascertain, this is the first usage of mixup to merge information from different paths. Our mixup is applied during autoencoding in two different stages, hence the term dual-mixup.

3. Method

To solve the tasks of clustering, foreground segmentation, and conditional generation with minimal supervision, our method trains multiple neural networks side-by-side. The sub-networks specialize in different sub-tasks, based on their architecture, relative position to the other networks, and a set of suitable losses. Each task is solved by applying the networks in a specific task-dependent path (Sec. 3.1).

In order to simplify training, instead of training the compound network to solve all three tasks at once, we schedule the training process by phases, see Sec. 4. The phases are designed to train the network for a gradually increasing subset of tasks, starting from image-level tasks (generating images) to semantic tasks (semantic segmentation of the foreground, and semantic clustering) that benefit from the capabilities obtained in the first phase.

The architecture of the compound model is depicted in Fig. 1 and Fig. 2 and the layers of the sub-networks are detailed in the appendix. Our solution consists of two generators, three encoders and two discriminators.

Generators The two generators run in parallel to produce an output image, where each generator captures a different aspect of the generated image. The generators are conditioned on a two-level hierarchical categorization. Each category has a unique child class ϕ_c and a parent class ϕ_p shared by multiple child classes. These classes are represented by the one-hot vectors (e_c, e_p). An additional background one-hot vector e_{bg} affects the generation of the background images. Since there is a tight coupling between the class of the object (water bird, tropical bird, etc.) and the expected background, the typology of the background follows the coarse hierarchy, i.e. the parent class.

$$e_c[i] = \delta_{i,\phi_c}, \quad e_p[i] = \delta_{i,\phi_p}, \quad e_{bg} = e_p \quad (1)$$

A fourth vector z is sampled from a multi-variate gaussian distribution to represent non-categorical features.

The background generator G_{bg} receives the background vector e_{bg} and z and produces a background image I_{bg} . The foreground generator G_{fg} , receives the parent vector e_p , child vector e_c and the same z used in the background generation and produces a foreground image I_{fg} and a foreground mask I_m . The generator is optimized such that all foreground images with the same e_p will have the same object shape and all images with the same e_c will have a similar object appearance. The latent vector z is implicitly conditioned to represent all non-categorical information, such as pose, orientation, size, etc. It is used in both the background and foreground generation, so that the images produced by both networks will merge into a coherent image.

The generators start by converting the one-hot vectors into code vectors, using a single fully connected layer, in other words, look up tables (LUT). Such an embedding is often used when working with categorical values.

$$v_{bg} = V_{bg}(e_{bg}), \quad v_p = V_p(e_p), \quad v_c = V_c(e_c) \quad (2)$$

The generators are then applied to produce the background image I_{bg} , the foreground image I_{fg} and the mixing mask I_m . Each generator is a composition of sub modules applied

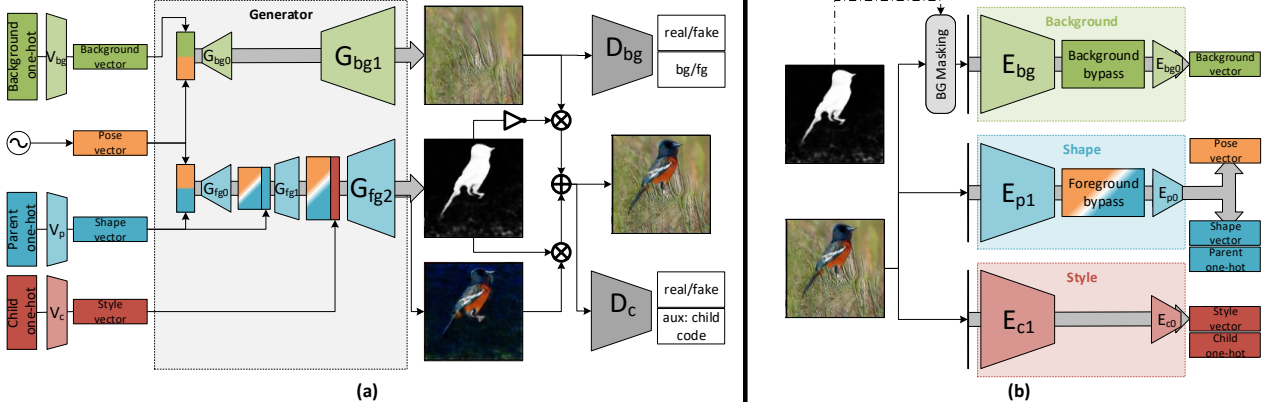


Figure 1. Flow of the generation path. (a) The generators decode the four priors (e_{bg} , e_p , e_c , z) and produce three separate images (foreground, background, mask) that are combined to the final image. (b) The generated image is encoded by three encoders to retrieve the latent variables and priors.

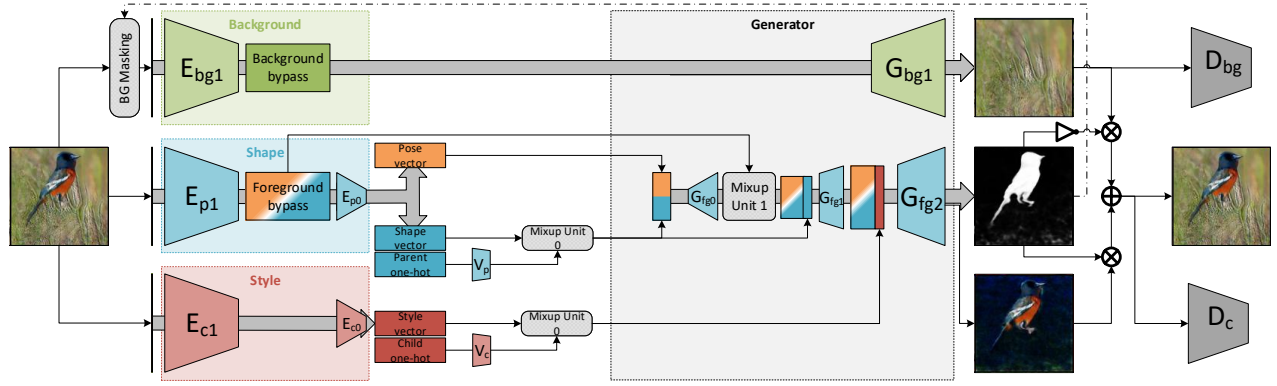


Figure 2. Flow of the reconstruction path introduced in Phase II of the training. The exact same sub-networks from Phase I are rearranged to produce an autoencoding path. The image is first encoded with the shape and style encoders, which produce latent codes for the foreground generator. The foreground generator then decodes the code to produce the foreground image and mask. With the mask, the background encoder encodes the image and the background generator decodes it to generate a background image. The image is finally reconstructed from the combined images. Between the encoders and the generators, the predicted shape and style codes, and those produced by the LUT (V_p , V_c), are merged with a mixup module. Furthermore, the bypass tensor B_{bg} replaces the pre-image A_{bg} and the bypass B_{fg} is merged with the pre-image tensor A_{fg} as skip connections to improve the background mask generation and object shape representation.

back to back:

$$A_{bg} = G_{bg0}(v_{bg}, z) \quad (3)$$

$$I_{bg} = G_{bg1}(A_{bg}) \quad (4)$$

$$A_{fg} = G_{fg0}(v_p, z) \quad (5)$$

$$(I_{fg}, I_m) = G_{fg2}(G_{fg1}(A_{fg}, v_p), v_c) \quad (6)$$

During autoencoding, the interface of the generators changes, due to the bypasses (B_{bg} , B_{fg}) and the mixup module. Instead of A_{bg} , B_{bg} is passed, and instead of (v_c, v_p, A_{fg}) we pass $(v_{cmix}, v_{pmix}, A_{fgmix})$, as described in Eq. 16.

The final generated image is:

$$I = I_{bg} \circ (1 - I_m) + I_{fg} \circ I_m, \quad (7)$$

where \circ denotes an element-wise multiplication.

Encoders Unlike FineGAN, our framework requires the use of encoders. There are three matching encoders: the

background encoder E_{bg} , the content encoder E_p , and the style encoder E_c . They run in semi-parallel to predict both the latent codes (v_{bg} , v_p , v_c , z) of an input image and the underlying one-hot vectors (e_{bg} , e_p , e_c). All encoders are fed with image I as input and the background encoder is also fed with the mask I_m . Since there is no annotated mask, the mask is produced according to Eq. 6 by the foreground generator, when fed by the encoding produced by the content and style encoders.

$$(\hat{e}_p, \mu_p, \sigma_p, B_{fg}, \mu_z, \sigma_z) = E_p(I) \quad (8)$$

$$(\hat{e}_c, \mu_c, \sigma_c) = E_c(I) \quad (9)$$

$$(B_{bg}) = E_{bg}(I, I_m) \quad (10)$$

where (\hat{e}_p, \hat{e}_c) are prediction probabilities for the parent and child classes, (μ, σ) are vectors of sizes (d_z, d_p, d_c) defining the mean and variance to sample each element of $(\hat{z}, \hat{v}_p, \hat{v}_c)$ from a gaussian distribution, (B_{bg}, B_{fg}) are the bypasses

depicted in Fig. 2 as skip connections between encoders and generators.

Discriminators Following [23], the two discriminators are adversarial opponents on the outputs I_{bg}, I . The background discriminator D_{bg} receives either a real background image from the set X_{bg} , a fake background image generated by the background generator, or a real object image from the set X_c . This discriminator has three tasks, with a separate output for each. The tasks are as follows: (i) patch-wise prediction if the input image is real or fake, annotated as D_{bgA} . (ii) patch-wise prediction if the input image is a background image or not, annotated as D_{bgB} . (iii) extract hidden layer output for the perceptual loss, annotated as D_{bgC} .

The image discriminator D_c receives real images from X_c or generated fake images, and also has three tasks: (i) predict if the input image is real or fake, annotated as D_{cA} . (ii) predict the child class ϕ_c of the image, annotated as D_{cB} . (iii) extract hidden layer output for perceptual loss, annotated as D_{cC} . The classification task is not an adversarial one, and the foreground generator is cooperating with that task, instead of aiming to fool it. The first and third tasks lead the generators to generate real looking images and the second task encourages the generators to condition the generation on the child class.

During training, when entering Phase II, the fake images for both discriminators can be a result of either (i) the generation path, (ii) fake image autoencoding, or (iii) real image autoencoding. These paths can generate very different images and the discriminators might not be able to optimize them simultaneously since, each path is practically a different domain. We noticed that images from the autoencoding path fail to converge to real-looking images when the discriminators are trained only by the generation path outputs. To solve this, upon entering Phase II, we clone each discriminator (D_c, D_{bg}) twice and associate one separate clone for each path, resulting in a total of three background discriminators and another three for the foreground. In this setting, each path receives the adversarial signal that is concentrated at improving the results in that particular path.

3.1. Inference tasks

For **image generation**, the input is a set of vectors (e_{bg}, e_p, e_c, z) . The path is described in Fig. 1, Eq. 2–7.

For **image autoencoding**, the input is an image I . The path is described in Fig. 2. The precise flow is: (1) encode the foreground through the content and style encoders (E_p, E_c) , Eq. 8,9, (2) generate a foreground image and mask with the foreground generator G_{fg} , Eq. 6, (3) encode the image and mask through the background encoder E_{bg} , Eq. 10, (4) generate the background image with the background generator G_{bg} , Eq. 4, and (5) compose the final image with (I_{fg}, I_{bg}, I_m) , Eq. 7. The background encoding is delayed, because it relies on a segmentation mask which

has to be generated first.

For **segmentation**, the input is an image I . The path is the same as steps (1-2) in the autoencoding task. The segmentation mask is the produced foreground mask I_m .

For **clustering**, the input is the image I . The clusters are acquired by applying the content and style encoders (E_p, E_c) and use the prediction of the parent and child classes for hierarchical clustering or only the child class for non-hierarchical clustering. The clusters can be determined by the predicted one-hot vectors (e_p, e_c) , but better results, and the ones shown in the evaluation section, were reached when applying the K-means algorithm on the concatenated code vectors $[v_p, v_c]$.

4. Multi-phase training

Without a multi-phase training, the networks would train to generate fake images and autoencode real and fake images simultaneously. While the generation flow encourages a separation between the background and foreground components, the autoencoding flow resists this separation due to the trivial solution of encoding and decoding the image in one of the paths (foreground or background) and applying an all-zero or all-one mask.

The multi-phase training has two phases. In the first phase, we train the generators to synthesize images conditioned on latent variables, while considering the background and the foreground separately. In this controlled environment, the generators are much more likely to converge to the required setting and in less training iterations. After a decent amount of iterations, determined in advance by a hyperparameter, the second phase kicks in, where (i) the model is trained to also reconstruct images through both latent variables and bypass information from the encoders, and (ii) the information from the encoders and the information from the latent vectors are merged with the mixup module at two separate locations independently.

4.1. Phase I of training

In the first phase of training, the model learns to generate images I in a way that relies on generating a background image I_{bg} , a foreground image I_{fg} , and a foreground mask I_m , as in Fig. 3. The discriminators are trained along with the generators and produce an adversarial training signal. The encoders are also trained in this phase, but only to retrieve the latent variables from the generated images.

The losses in Phase I can be put into four groups: adversarial losses, classification losses, distance losses, and regularizations. For brevity, e represents the dependence on the three prior codes (e_{bg}, e_p, e_c) . Similarly, $G(e, z)$ represents the full generation of the final image, Eq. 3–7.

Adversarial losses These involve the two discriminators and are derived from the minimax equation: $\min_G \max_D \mathbb{E}_x[\log(D(x))] + \mathbb{E}_z[\log(1 - D(G(z)))]$, for

a generic generator G and discriminator D . The concrete GAN loss is the sum of the losses for the separation between real/fake background, the separation between background/object and the separation between real/fake object.

For the generators, the losses are:

$$\begin{aligned}\mathcal{L}_{G_{bgA}} &= \mathbb{E}_{e_{bg}, z} [\log(D_{bgA}(G_{bg}(e_{bg}, z)))] \\ \mathcal{L}_{G_{bgB}} &= \mathbb{E}_{e_{bg}, z} [\log(D_{bgB}(G_{bg}(e_{bg}, z)))] \\ \mathcal{L}_{G_{cA}} &= \mathbb{E}_{e, z} [\log(D_{cA}(G(e, z)))] \\ \mathcal{L}_G &= 10 \cdot \mathcal{L}_{G_{bgA}} + \mathcal{L}_{G_{bgB}} + \mathcal{L}_{G_{cA}}\end{aligned}\quad (11)$$

For the discriminators, where X_{bg} , X_c are the sets of real background images and real object images, the losses are:

$$\begin{aligned}\mathcal{L}_{D_{bgA}} &= \mathbb{E}_{x \sim X_{bg}} [\log(D_{bgA}(x))] + \\ &\quad \mathbb{E}_{e_{bg}, z} [\log(1 - D_{bgA}(G_{bg}(e_{bg}, z)))] \\ \mathcal{L}_{D_{bgB}} &= \mathbb{E}_{x \sim X_{bg}} [\log(D_{bgB}(x))] + \\ &\quad \mathbb{E}_{x \sim X_c} [\log(1 - D_{bgB}(x))] \\ \mathcal{L}_{D_{cA}} &= \mathbb{E}_{x \sim X_c} [\log(D_{cA}(x))] + \\ &\quad \mathbb{E}_{e, z} [\log(1 - D_{cA}(G(e, z)))] \\ \mathcal{L}_D &= 10 \cdot \mathcal{L}_{D_{bgA}} + \mathcal{L}_{D_{bgB}} + \mathcal{L}_{D_{cA}}\end{aligned}\quad (12)$$

Classification losses These losses optimize the generators to generate distinguished images for each style and shape prior and the encoders to retrieve the prior classes.

$$\mathcal{L}_E = \text{CE}(D_{cB}(I), \phi_c) + \text{CE}(\hat{e}_p, \phi_p) + \text{CE}(\hat{e}_c, \phi_c), \quad (13)$$

where CE is the cross entropy loss, and D_{cB} is the conditional task of the discriminator described in Sec. 3. \hat{e}_p, \hat{e}_c are class predictions from Eq. 8,9 and ϕ_c, ϕ_p are the child and parent classes the image was generated with, Eq. 1.

Distance losses We train the encoders to minimize the mean squared error between the vectors in the latent space produced during generation and their predicted counterparts. These vectors are used in the next phase to feed the generator in the autoencoding path, making it beneficial to add this constraint already at this phase.

$$\begin{aligned}\mathcal{L}_{\text{MSE}} &= \text{MSE}(\mathbf{v}_c, \boldsymbol{\mu}_c) + \text{MSE}(\mathbf{v}_p, \boldsymbol{\mu}_p) + \\ &\quad \text{MSE}(A_{fg}, B_{fg}) + \text{MSE}(A_{bg}, B_{bg}),\end{aligned}\quad (14)$$

where $A_{bg}, A_{fg}, B_{bg}, B_{fg}$ are the "pre-image" and "bypass" tensors, computed by Eq. 3,5,8,10, and $\boldsymbol{\mu}_c, \boldsymbol{\mu}_p$ are the mean vectors to sample the latent code ($\hat{\mathbf{v}}_c, \hat{\mathbf{v}}_p$) with.

Regularization losses For regularization, a loss term is applied on the latent codes ($\mathbf{v}_{bg}, \mathbf{v}_p, \mathbf{v}_c$), annotated as $\mathcal{L}_{\text{REG}_v}$, and on the foreground mask I_m , annotated as \mathcal{L}_M . They are detailed in the appendix.

All the losses are summed together to the total loss:

$$\mathcal{L}_{\text{GEN}} = \mathcal{L}_E + \mathcal{L}_{\text{MSE}} + 0.1 \cdot \mathcal{L}_{\text{REG}_v} + \mathcal{L}_G + 2 \cdot \mathcal{L}_M \quad (15)$$

4.2. Phase II of training

In the second phase of the training, an additional task is added, where the network has to utilize the encoders and generators to reconstruct an input image, as in Fig. 4. To

each batch iteration, two new reconstruction paths are performed, where the input image can be either a real image, or a fake image generated from latent code in advance. To smooth the transition for sole image generation to multi-task state, we begin with only reconstructing fake images, which the model is already familiar with, and delay the real image reconstruction with a hyperparameter. We have also found that starting with only training the encoders and keeping the generators fixed in the first iterations of this phase also assists in this transition.

This phase is also when the mixup is introduced. The application of mixup in our setting serves two purposes in two separate locations inside the compound network, hence the term dual mixup.

The first mixup (mixup0 in Fig. 2) mixes the vectors ($\hat{\mathbf{v}}_p, \hat{\mathbf{v}}_c$) provided by the encoders E_p, E_c with the one-hot vector embeddings ($\mathbf{v}_p, \mathbf{v}_c$) given by the LUT for the one-hot vectors ($\mathbf{e}_p, \mathbf{e}_c$). When fine-tuning the embeddings towards real image classes, we want to reduce the distance between the two matching vectors. Therefore, we merge the two types of vectors with the mixup module, such that both are part of the reconstruction and both will be optimized during the back-propagation.

The second mixup (mixup1 in Fig. 2) mixes the bypass B_{fg} with the pre-image A_{fg} . It serves to create the condition where the reconstruction path will be simultaneously dependent on the foreground bypass and on the lower stage of the foreground generator. In contrast to regular residual connections, the ever changing β used in the mixup forces the bypass and the pre-image to be independent representations and not complement each other. This way, at any time we can choose any β or even pass only the bypass or only the pre-image and result in an almost identical image.

Given two inputs and a parameter $\beta_i \in [0, 1]$, $i = 0, 1$. The mixup is defined as follows:

$$\begin{aligned}\mathbf{v}_{p_{mix}} &= \mathbf{v}_p \circ (1 - \beta_0) + \hat{\mathbf{v}}_p \circ \beta_0 \\ \mathbf{v}_{c_{mix}} &= \mathbf{v}_c \circ (1 - \beta_0) + \hat{\mathbf{v}}_c \circ \beta_0 \\ A_{fg_{mix}} &= A_{fg} \circ (1 - \beta_1) + B_{fg} \circ \beta_1,\end{aligned}\quad (16)$$

where $\beta_0 \in [0, 1], \beta_1 \in [0.5, 1]$ are randomly sampled in each iteration for each instance in the batch. When mixup is applied, the mixed features ($\mathbf{v}_{p_{mix}}, \mathbf{v}_{c_{mix}}, A_{fg_{mix}}$) replace the pre-mixup features ($\mathbf{v}_p, \mathbf{v}_c, A_{fg}$) as inputs to the generator, see Eq. 5,6.

The losses in this phase can be put in three groups: statistical losses, reconstruction losses, and perceptual losses.

Statistical losses As in Variational Auto-Encoders [16], we compare the Kullback-Leiber Divergence between the latent variables encoded by the encoders ($\hat{\mathbf{v}}_p, \hat{\mathbf{v}}_c, \hat{\mathbf{z}}$) to a multivariate gaussian distribution. For the pose vector \mathbf{z} , we used the standard normal distribution with covariance matrix equal to the identity matrix ($\Sigma = I_{d_z}$) and a zero mean vector ($\boldsymbol{\mu} = \mathbf{0}$). For the shape and style vectors ($\hat{\mathbf{v}}_p, \hat{\mathbf{v}}_c$) we

Model	Birds		Dogs		Cars	
	C-IS	NMI	C-IS	NMI	C-IS	NMI
Dataset	47.96	.738	77.13	.879	55.47	.626
StackGANv2	15.06	.171	10.24	.137	13.39	.167
FineGAN	24.75	.454	15.71	.403	13.67	.228
OneGAN	30.73	.541	19.66	.516	18.24	.275
w/o real recon	25.67	.499	17.03	.463	15.54	.288
Phase I only	21.65	.488	16.86	.443	13.42	.245
no multi-phase	2.30	.101	1.79	.158	3.93	.092

Table 1. Quantitative generation results.

still use identity Σ , but since they should match their latent code ($\mathbf{v}_p, \mathbf{v}_c$), we use these latent codes as the target mean.

$$\begin{aligned}
\mathcal{L}_{\text{VAE}_p} &= D_{\text{KL}}(\mathcal{N}(\boldsymbol{\mu}_p, \text{diag}(\sigma_p)) \| \mathcal{N}(\mathbf{v}_p, I_{d_p})) \\
\mathcal{L}_{\text{VAE}_c} &= D_{\text{KL}}(\mathcal{N}(\boldsymbol{\mu}_c, \text{diag}(\sigma_c)) \| \mathcal{N}(\mathbf{v}_c, I_{d_c})) \\
\mathcal{L}_{\text{VAE}_z} &= D_{\text{KL}}(\mathcal{N}(\boldsymbol{\mu}_z, \text{diag}(\sigma_z)) \| \mathcal{N}(\mathbf{0}, I_{d_z})) \\
\mathcal{L}_{\text{VAE}} &= \mathcal{L}_{\text{VAE}_p} + \mathcal{L}_{\text{VAE}_c} + \mathcal{L}_{\text{VAE}_z}
\end{aligned} \quad (17)$$

Reconstruction losses The reconstruction losses are a set of L1 losses that compare the difference between the input image to the output. The network trains at autoencoding both real and fake images. For fake images, we compare reconstruction of the full image, background image, and mask. For real images, the only ground-truth is the full image, so the loss only compares that.

$$\mathcal{L}_{\text{REC}} = \begin{cases} \text{L1}(I, \hat{I}) & , \text{real} \\ \text{L1}(I, \hat{I}) + \text{L1}(I_{bg}, \hat{I}_{bg}) + \text{L1}(I_m, \hat{I}_m) & , \text{fake} \end{cases}$$

Perceptual losses Comparing images to their ground-truth counterpart has been shown to produce blurred images; Perceptual loss [12] is known to aid in producing sharper images with more visible context [32]. The perceptual loss is often used along with a pre-trained network, but this relies on an image-net scale type of added supervision. In our case, we use the discriminators, which were pre-trained in the first phase. We use the notation D_{cc}, D_{bgc} from Sec. 3 to describe the networks used to extract the hidden layers before the output of the discriminators.

$$\mathcal{L}_{\text{PER}} = \begin{cases} \text{L2}_{D_{cc}}(I, \hat{I}) & , \text{real} \\ \text{L2}_{D_{cc}}(I, \hat{I}) + \text{L2}_{D_{bgc}}(I_{bg}, \hat{I}_{bg}) & , \text{fake} \end{cases}$$

where $\text{L2}_D(I_1, I_2) = \|D(I_1) - D(I_2)\|^2$.

All the losses are summed together to the total loss:

$$\mathcal{L}_{\text{AE}} = \mathcal{L}_{\text{GEN}} + \mathcal{L}_{\text{VAE}} + \mathcal{L}_{\text{REC}} + \mathcal{L}_{\text{PER}} \quad (18)$$

5. Experiments

We train the network for 600,000 iterations, with batch size 20. All sub-networks are optimized using Adam [15], with $\text{lr}=2\text{e-}4$ and default arguments. Phase I duration is 200,000 iterations. Within Phase II, we start with training

Model	Birds			Dogs		
	(i)	(ii)	(iii)	(i)	(ii)	(iii)
StackGANv2	6.3	1.4	5.7	3.5	1.5	5.2
FineGAN	6.0	5.0	7.0	5.8	4.4	8.2
OneGAN (ours)	7.3	6.9	8.7	6.8	6.4	8.3

Table 2. User study results. Average score between 1 to 10, for each question asked in the study. (i) overall quality (ii) conditional resemblance (iii) pose disentanglement

Model	Birds		Dogs		Cars	
	IOU	DICE	IOU	DICE	IOU	DICE
ReDO	46.5	60.2	38.4	52.8	16.2	26.2
UISB*	44.2	60.1	62.7	75.5	64.7	77.5
IIC stuff-3*	36.5	70.2	58.5	71.5	58.5	71.5
IIC stuff*	35.2	50.4	56.6	70.2	58.8	71.7
OneGAN	55.5	69.2	71.0	81.7	69.7	81.0
w/o real recon	53.5	67.7	67.1	78.6	69.8	81.1
Phase I only	45.7	60.6	65.1	77.3	64.8	75.9
no multi-phase	28.2	43.2	7.4	13.6	45.9	60.5

Table 3. Segmentation results. *unfair upper bound results, obtained by selecting the best result out of many.

Model	Birds		Dogs		Cars	
	NMI	AMI	NMI	AMI	NMI	AMI
JULE [†]	.204	—	.142	—	.232	—
DEPICT [†]	.290	—	.182	—	.329	—
IIC	.345	.106	.200	.127	.254	.056
StackGANv2	.253	.073	.139	.075	.174	.025
FineGAN	.349	.152	.194	.122	.233	.055
OneGAN (ours)	.391	.173	.202	.129	.266	.071
w/o real recon	.389	.171	.194	.121	.250	.066
Phase I only	.352	.151	.175	.100	.244	.063
no multi-phase	.216	.024	.082	.021	.208	.013

Table 4. Clustering results. [†]provided by [23] without AMI.

only on fake images and real image reconstruction starts after another 200,000 iterations.

We evaluate our model on various tasks against the state of the art methods. Since no other model can solve all these tasks, we evaluate against different methods in each task. Depending on availability, some baselines were pre-trained models released by the authors and some were trained from scratch with the authors’ code.

Datasets We evaluate our model with three datasets of fine-grained categorization. **Caltech-UCSD Birds-200-2011 (Birds)** [25]: This dataset consists of 11,788 images of 200 classes of birds, annotated with bounding boxes and segmentation masks. **Stanford Dogs (Dogs)** [17]: This dataset consists of 20,580 images of 120 classes of dogs, annotated with bounding boxes. For evaluation, target segmentation masks were generated by a pre-trained

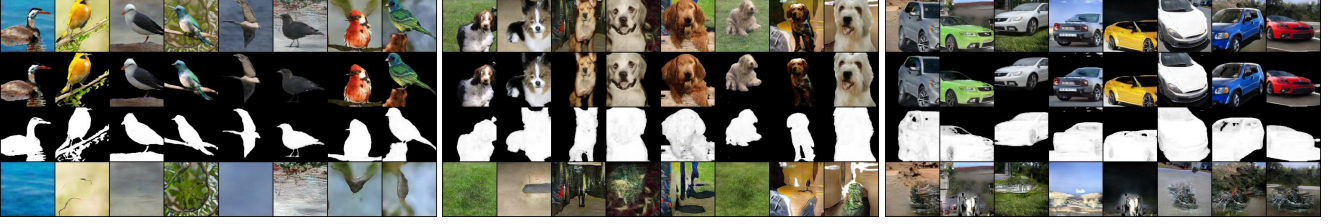


Figure 3. Image Generation for each dataset. From top to bottom: (i) final image, (ii) foreground, (iii) foreground mask, (iv) background.

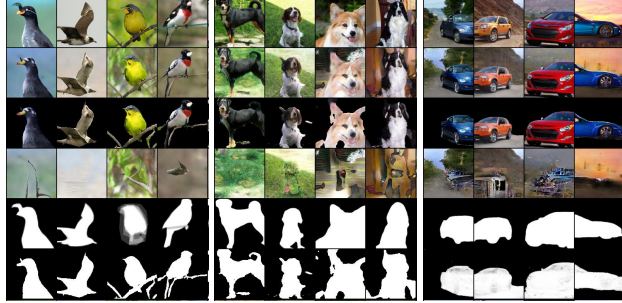


Figure 4. Image reconstruction for each dataset. From top to bottom: (i) real image, (ii) reconstructed image, (iii) reconstructed foreground, (iv) reconstructed background, (v) ground-truth foreground mask, (vi) predicted foreground mask.

DeepLabV3 [3] model on the COCO [19] dataset. The pre-trained model was acquired from the gluoncv toolkit [10]. **Stanford Cars (Cars)** [14]: This dataset consists of 16,185 images of 196 classes of cars, annotated with bounding boxes. Segmentation masks were generated as above with the pre-trained DeepLabV3 model.

For all datasets, to produce an object and background subsets X_c, X_{bg} , we split the dataset in a 80/20 ratio. We take the bigger subset for X_c . Out of the smaller subset, we use the bounding boxes to cut background patches to use as background images. No image was used for both foreground and background examples and, of course, the bounding boxes were not used to train our method.

Due to the different size of classes in each dataset, there is also a different size of child and parent classes in the design for each dataset. Birds: $N_C = 200, N_P = 20$, Dogs: $N_C = 120, N_P = 12$, Cars: $N_C = 196, N_P = 14$.

Conditional image generation We compare our image generation results to FineGAN [23] and StackGANv2 [31], by relying on an InceptionV3 fine-tuned on each dataset. The normalized mutual information (NMI) between the child classes and the classes predicted by the Inception model is employed. In addition, we perform a conditional variation (C-IS) of the Inception Score [22] (IS). For each child class, we average the predictions of the Inception model, and compute the IS on the class average. Following the same principle as the original IS evaluation, a good model should have high a probability on a single real class for each conditioned child class and a uniform distribution across all classes when averaged across all child classes.

Our results, reported in Tab. 1 show that OneGAN out-

performs in both conditional image generation metrics. StackGANv2 was the worst performing model, which suggests that mask-based generation used by our model and by FineGAN is very useful for conditional generation. Our model also outperformed FineGAN, which as our ablation demonstrates, is due to the added reconstruction path during training. We back these numerical results with Fig. 5.

We strengthen these results with a user study. In the study, we chose ten different real images. For each model (OneGAN, FineGAN, StackGANv2), we encoded the images to extract the image child and parent code and then produced ten images conditioned on the codes of each of the ten images (see supplementary for the images). We then asked the following questions: (i) How realistic do the images look? (ii) How much are the objects in the images related to the conditioned images? (iii) How are images generated by the same z show the same non-categorical similarity (pose, size, location, etc.). As in the results, presented in Tab. 2 show, our model generates conditioned images that are of better quality and represent a more coherent class. Our model also disentangles the categorical and non-categorical features better than the other models.

Unsupervised foreground segmentation We compare our mask prediction from the autoencoding pathway to the real foreground mask. We evaluate according to IOU and DICE scores. We compare against two baselines, ReDO [4] and UISB [13] which are trained for each dataset separately, and a third one, IIC [11], which was trained on coco-stuff and coco-stuff-3 (a subset). While coco-stuff is a different dataset than the ones we used, it contains all the relevant classes. ReDO produces a foreground which we compare to the ground-truth similarly to how we evaluate our model. UISB is an iterative method that produces a final segmentation with a varying number of classes between 2 and 100. We iterated UISB on each image 50 times. The output was usually between 4-20 classes. Since there is no labeling of the foreground or background classes, this method cannot be immediately used for this task. In order to get an evaluation, we look for each image for the class that has the highest IOU with the ground-truth foreground. The rest of the classes are merged to a single background class. We then repeat with a single background class and the rest merged into foreground. Finally, taking the best out of the two options, each obtained by using an oracle to select out of many

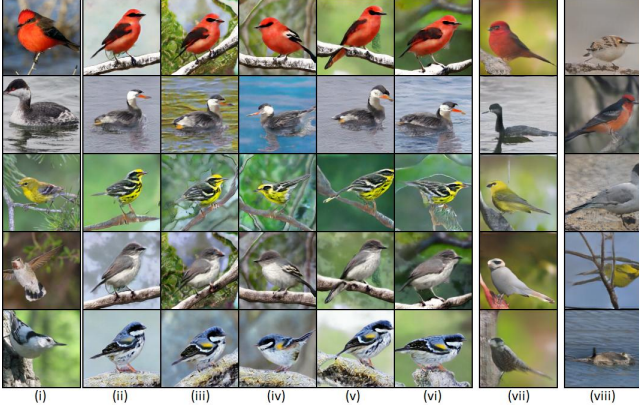


Figure 5. Conditional Generation. From left to right: (i) real images, (ii-vi) generation of images with the encoded parent and child codes and a different vector z per column, (vii) FineGAN [23] results, (viii) StackGANv2 [31] results.

options, which provides a liberal upper bound on the performance of UIBS. IIC also produces a multi-class segmentation map, we use it in the same way we use UIBS by taking the best class for either background or foreground in respect to IOU. IIC has 2-headed output, one for the main task and one for over-clustering. For coco-stuff trained IIC, we look for the best mask in one of the 15 classes of the main head. For coco-stuff-3 trained IIC, the main head is trained to cluster sky/ground/plants, so we look for the best mask in one of the 15 classes of the over-clustering head. The results in Table. 3 show that our method outperforms all the baselines. The generated masks are presented in Fig. 4.

Unsupervised clustering We compare our model against our encoders trained alongside StackGANv2 and FineGAN. Similarly to our model, we trained a child and parent encoders for both models during training. In this task, we evaluate how well the encoders are capable of clustering real images. We also compare our model against other clustering methods: JULE [29], DEPICT [8] and IIC [11].

The results show that our model outperforms the other models for both Birds and Dogs datasets. For the Cars dataset, similarly to the generation results, our model and other models as well, grouped images more on the basis of color than car model. This caused a reduced performance in clustering, and our model was only second best.

Object removal and inpainting Through the reconstruction task, our model is also capable of performing automatic object removal and background reconstruction, see Fig. 4. In contrast to other known method for inpainting, due to the lack of perfect ground-truth mask, our model does not only fill the missing pixels but fully reconstructs the background image. As a result, the background image is not identical to the original background, but it is semantically similar to it. See supplementary for a comparison with previous work.

Image to image translation To further evaluate our

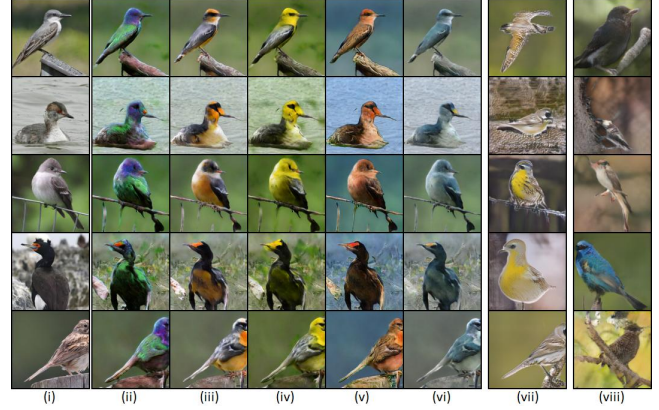


Figure 6. Style Transfer. From left to right: (i) real images. (ii-vi) reconstructed images when the child code e_c is switched with a code from a selected category, (vii) FineGAN [23] results, (viii) StackGANv2 [31] results.

model, we show its capability to transfer an input image to a target category. The results can be seen in Fig. 6. Even though our model was never trained on this task, the disentanglement between the shape and the texture enables this task simply by passing a different child code during reconstruction. By selecting different child codes, we can manipulate the appearance of the object to any of the child categories. In contrast, FineGAN and StackGANv2 are unable to perform this task correctly as there is no learned disentanglement in StackGAN’s case and no bypass connection in FineGAN’s case to allow good reconstruction.

Ablation study In Tab. 1, 3 and 4, we provide multiple versions of our method for ablation. In the version without real reconstruction, we only add fake image reconstruction in Phase II, meaning that real images did not pass through the network during training. Another variant employs only the first phase of training. Finally, a third variant trains all losses at once, without multi-phase training. In addition, in the supplementary, we provide an ablation study supporting mixup, bypass connections, and various loss terms.

6. Conclusions

By building a single model to handle multiple unsupervised tasks at once, we convincingly demonstrate the power of co-training, by surpassing the performance of the best in class methods for each task. This capability is enabled by a complex architecture with many sub-networks. Considering biological visual system, one can expect future architectures to be complex and to contain multiple pathways between the various modules. However, supporting this complexity during training is challenging. We introduce a dual mixup loss that integrates multiple pathways in a homogenized manner and a multi-phase training, which helps to avoid some tasks dominating over the others.

Acknowledgement

This project has received funding from the European Research Council (ERC) under the European Unions Horizon 2020 research and innovation programme (grant ERC CoG 725974).

References

- [1] Jimmy Lei Ba, Jamie Ryan Kiros, and Geoffrey E Hinton. Layer normalization. *arXiv preprint arXiv:1607.06450*, 2016. 2
- [2] Liang-Chieh Chen, George Papandreou, Iasonas Kokkinos, Kevin Murphy, and Alan L Yuille. Deeplab: Semantic image segmentation with deep convolutional nets, atrous convolution, and fully connected crfs. *IEEE transactions on pattern analysis and machine intelligence*, 40(4):834–848, 2017. 2
- [3] Liang-Chieh Chen, George Papandreou, Florian Schroff, and Hartwig Adam. Rethinking atrous convolution for semantic image segmentation. *arXiv preprint arXiv:1706.05587*, 2017. 2, 7
- [4] Mickaël Chen, Thierry Artières, and Ludovic Denoyer. Unsupervised object segmentation by redrawing. *arXiv preprint arXiv:1905.13539*, 2019. 2, 7
- [5] Xi Chen, Yan Duan, Rein Houthoofd, John Schulman, Ilya Sutskever, and Pieter Abbeel. Infogan: Interpretable representation learning by information maximizing generative adversarial nets. In *Advances in neural information processing systems*, pages 2172–2180, 2016. 1
- [6] Ioana Croitoru, Simion-Vlad Bogolin, and Marius Leordeanu. Unsupervised learning of foreground object detection. *arXiv preprint arXiv:1808.04593*, 2018. 2
- [7] Yann N Dauphin, Angela Fan, Michael Auli, and David Grangier. Language modeling with gated convolutional networks. In *Proceedings of the 34th International Conference on Machine Learning-Volume 70*, pages 933–941. JMLR.org, 2017. 2
- [8] Kamran Ghasedi Dizaji, Amirhossein Herandi, Cheng Deng, Weidong Cai, and Heng Huang. Deep clustering via joint convolutional autoencoder embedding and relative entropy minimization. In *Proceedings of the IEEE International Conference on Computer Vision*, pages 5736–5745, 2017. 2, 8
- [9] Ian Goodfellow, Jean Pouget-Abadie, Mehdi Mirza, Bing Xu, David Warde-Farley, Sherjil Ozair, Aaron Courville, and Yoshua Bengio. Generative adversarial nets. In *Advances in neural information processing systems*, pages 2672–2680, 2014. 1
- [10] Jian Guo, He He, Tong He, Leonard Lausen, Mu Li, Haibin Lin, Xingjian Shi, Chenguang Wang, Junyuan Xie, Sheng Zha, Aston Zhang, Hang Zhang, Zhi Zhang, Zhongyue Zhang, and Shuai Zheng. Gluoncv and gluonnlp: Deep learning in computer vision and natural language processing. *arXiv preprint arXiv:1907.04433*, 2019. 7
- [11] Xu Ji, João F Henriques, and Andrea Vedaldi. Invariant information clustering for unsupervised image classification and segmentation. In *Proceedings of the IEEE International Conference on Computer Vision*, pages 9865–9874, 2019. 2, 7, 8
- [12] Justin Johnson, Alexandre Alahi, and Li Fei-Fei. Perceptual losses for real-time style transfer and super-resolution. In *European Conference on Computer Vision*, pages 694–711. Springer, 2016. 6
- [13] Asako Kanezaki. Unsupervised image segmentation by backpropagation. In *2018 IEEE International Conference on Acoustics, Speech and Signal Processing (ICASSP)*, pages 1543–1547. IEEE, 2018. 2, 7
- [14] Aditya Khosla, Nityananda Jayadevaprakash, Bangpeng Yao, and Li Fei-Fei. Novel dataset for fine-grained image categorization. In *First Workshop on Fine-Grained Visual Categorization, IEEE Conference on Computer Vision and Pattern Recognition*, Colorado Springs, CO, June 2011. 7
- [15] D.P. Kingma and J. Ba. Adam: A method for stochastic optimization. In *The International Conference on Learning Representations (ICLR)*, 2016. 6
- [16] Diederik P Kingma and Max Welling. Auto-encoding variational bayes. *stat*, 1050:1, 2014. 1, 5
- [17] Jonathan Krause, Michael Stark, Jia Deng, and Li Fei-Fei. 3d object representations for fine-grained categorization. In *4th International IEEE Workshop on 3D Representation and Recognition (3dRR-13)*, Sydney, Australia, 2013. 6
- [18] Anders Boesen Lindbo Larsen, Søren Kaae Sønderby, Hugo Larochelle, and Ole Winther. Autoencoding beyond pixels using a learned similarity metric. *arXiv preprint arXiv:1512.09300*, 2015. 1
- [19] Tsung-Yi Lin, Michael Maire, Serge Belongie, James Hays, Pietro Perona, Deva Ramanan, Piotr Dollár, and C Lawrence Zitnick. Microsoft coco: Common objects in context. In *European conference on computer vision*, pages 740–755. Springer, 2014. 7
- [20] Mehdi Mirza and Simon Osindero. Conditional generative adversarial nets. *arXiv preprint arXiv:1411.1784*, 2014. 1
- [21] O. Ronneberger, P. Fischer, and T. Brox. U-net: Convolutional networks for biomedical image segmentation. In *Medical Image Computing and Computer-Assisted Intervention (MICCAI)*, volume 9351 of *LNCS*, pages 234–241. Springer, 2015. (available on arXiv:1505.04597 [cs.CV]). 2
- [22] Tim Salimans, Ian J. Goodfellow, Wojciech Zaremba, Vicki Cheung, Alec Radford, and Xi Chen. Improved techniques for training gans. *arXiv preprint arXiv:1606.03498*, 2016. 7
- [23] Krishna Kumar Singh, Utkarsh Ojha, and Yong Jae Lee. Finegan: Unsupervised hierarchical disentanglement for fine-grained object generation and discovery. *arXiv preprint arXiv:1811.11155*, 2018. 2, 4, 6, 7, 8
- [24] Maryam Sultana, Arif Mahmood, Sajid Javed, and Soon Ki Jung. Unsupervised deep context prediction for background estimation and foreground segmentation. *Machine Vision and Applications*, 30(3):375–395, 2019. 2
- [25] C. Wah, S. Branson, P. Welinder, P. Perona, and S. Belongie. The Caltech-UCSD Birds-200-2011 Dataset. Technical Report CNS-TR-2011-001, California Institute of Technology, 2011. 6
- [26] Jingdong Wang, Ke Sun, Tianheng Cheng, Borui Jiang, Chaorui Deng, Yang Zhao, Dong Liu, Yadong Mu, Mingkui

Tan, Xinggang Wang, et al. Deep high-resolution representation learning for visual recognition. *arXiv preprint arXiv:1908.07919*, 2019. 2

- [27] Ye Wang, Jongmoo Choi, Yueru Chen, Siyang Li, Qin Huang, Kaitai Zhang, Ming-Sui Lee, and C-C Jay Kuo. Un-supervised video object segmentation with distractor-aware online adaptation. *arXiv preprint arXiv:1812.07712*, 2018. 2
- [28] Xide Xia and Brian Kulis. W-net: A deep model for fully unsupervised image segmentation. *arXiv preprint arXiv:1711.08506*, 2017. 2
- [29] Jianwei Yang, Devi Parikh, and Dhruv Batra. Joint unsupervised learning of deep representations and image clusters. In *Proceedings of the IEEE Conference on Computer Vision and Pattern Recognition*, pages 5147–5156, 2016. 2, 8
- [30] Hongyi Zhang, Moustapha Cisse, Yann N Dauphin, and David Lopez-Paz. mixup: Beyond empirical risk minimization. *arXiv preprint arXiv:1710.09412*, 2017. 2
- [31] Han Zhang, Tao Xu, Hongsheng Li, Shaoting Zhang, Xiaogang Wang, Xiao lei Huang, and Dimitris N Metaxas. Stackgan++: Realistic image synthesis with stacked generative adversarial networks. *IEEE transactions on pattern analysis and machine intelligence*, 41(8):1947–1962, 2018. 7, 8
- [32] Richard Zhang, Phillip Isola, Alexei A Efros, Eli Shechtman, and Oliver Wang. The unreasonable effectiveness of deep features as a perceptual metric. In *Proceedings of the IEEE Conference on Computer Vision and Pattern Recognition*, pages 586–595, 2018. 6

A. Summary of notation

For convenience, in Tab. 5 we provide a complete listing of the notation used in our paper.

B. Regularization

Due to lack of space in the main text, we include the regularization loss terms as part of the supplementary.

During generation, we apply regularization on the latent vectors and on the mask image. The former serves to bound the range of the values to be close to the axis center and to be closely grouped.

$$\mathcal{L}_{REG_v} = ||v_p||_2^2 + ||v_c||_2^2 + ||v_{bg}||_2^2$$

The regularization on the mask serves to direct the model to utilize the mask efficiently, with a balanced and decisive representation of background and foreground. For mask batch $\mathbf{I}_m \in [0, 1]^{N, H, W}$, with N as the batch size and H, W the height and width of the mask. The first regularization term balances the mask value around the value of half.

$$\mathcal{L}_{M_B} = \frac{1}{N} \sum_n \left| \frac{1}{HW} \left(\sum_{i,j} (\mathbf{I}_m)_{n,i,j} \right) - \frac{1}{2} \right|$$

The second regularization term aims to make the masks more decisive. It is better described when the mask is between $[-1, 1]$ so we define $\mathbf{I}'_m = 2 \cdot \mathbf{I}_m - 1$. In the ideal

case, all pixels are either 1 or -1 (either background of foreground), therefore, if we assume a balanced distribution, for each mask the average value of $\max(0, \mathbf{I}'_m)$ is 0.5 and of $\min(0, \mathbf{I}'_m)$ it's -0.5, since half of the pixels are zeroed in each term. This is the decisiveness regularization.

$$\mathcal{L}_{M_D} = \frac{1}{N} \sum_n \left(\left| \frac{1}{HW} \left(\sum_{i,j} \max(0, (\mathbf{I}'_m)_{n,i,j}) \right) - \frac{1}{2} \right| + \left| \frac{1}{HW} \left(\sum_{i,j} \min(0, (\mathbf{I}'_m)_{n,i,j}) \right) + \frac{1}{2} \right| \right)$$

Together, the mask regularization loss is:

$$\mathcal{L}_M = \mathcal{L}_{M_B} + 0.1 \cdot \mathcal{L}_{M_D}$$

Both regularizations are added to the rest of the generation losses in Eq. 15.

C. Sub-networks architecture

In this section, we describe the details of each sub-network described in Sec. 3 and shown in Fig. 1,2. The layers of each sub-network are listed in the tables Tab. 7–13, with some modules that are frequently used listed in Tab. 6. The majority of the networks are sequential. When more complicated connections are present, the input and output notations are there to guide the flow.

C.1. GLU layer-normalization

Due to the training with a low batch size, having a large number of classes, and use of different paths, batch-normalization did not have a positive effect in our method. We experimented with many different alternatives, ranging from (i) layer-normalization, (ii) instance-normalization (iii) no normalization (iv) a combination of different normalization layers for each sub-network. We came to the conclusion that layer-normalization performed the best when used across all networks. Additionally, in the generators, where Gated Linear Unit (GLU) was used as non-linear activation, we realised that a more complex method needs to be applied. The GLU performs a non-linear activation function by splitting the input x in half on its channel axis, resulting in two equally sized tensors with half the number of channels as the input (x_R, x_L). One of the tensors then goes through a sigmoid activation and then multiplied by the other tensor to produce the output.

$$\text{GLU} : o = \text{sigmoid}(x_R) \circ x_L$$

By this implementation, if the tensor x is normalized with a layer-normalization, then x_R, x_L affect each other, and since they serve a different purpose in the normalization, it has an unwanted effect. To solve this, we separate the layers before the normalization, and apply the layer-normalization only on x_L .

$$\text{GLUNorm} : o = \text{sigmoid}(x_R) \circ \text{LayerNorm}(x_L)$$

D. A comprehensive ablation study

In the main paper, we address in Tab. 1,3,4, how different training methods affect on performance. We showed that applying image reconstruction at Phase II greatly improves the results in all tasks. Then, we also showed that applying not only fake image reconstruction, but also real image reconstruction, improves most of the results. Finally, we showed that the multi-phase training method is crucial by showing that a method trained without multi-phase performed very poor and, in fact, did not manage to learn any task.

The conclusion from these tests were that the use multi-phase helps the model to start learning the generation task first and then learn the reconstruction tasks on top of that learned skill. The ablation also showed that using the reconstruction task helped not only in segmentation and clustering, but also in the generation task itself, which does not use an image as input and is a task who's training has been started before the reconstruction was introduced.

In this section, we provide more ablation studies and make the further conclusions. In addition to the ablation results reported in the main text, we also show performance in both image generation and image segmentation on the birds dataset, see Table. 14. The supplementary ablation inspects the usage of mask regularization, bypass and mixup.

In our experiments, it is evident that mask regularization and limiting mixup1 to $\beta_1 \in [0.5, 1]$ improves the segmentation performance. Further, mask regularization, bypass and mixup all contribute to the conditional generation performance.

Specifically, mask regularization helps by distancing the model from the state that the generated masks are all-one or all-zero.

The bypass also contributes to both metrics. In the experiments we have seen that the reconstructed masks produced without bypass have an accurate coarse shape, but lack the fine details, therefore under-performing since the masks do not fit the object as well as with the bypass.

For the mixup module, we experimented with different variations of ranges for β_0, β_1 . (1) Without mixup at all, i.e. $\beta_0 = 1, \beta_1 = 1$, there is a full use of the bypass, but no use of the vectors from the LUT, this resulted in a high segmentation score since the bypass was still fully used, but with a low conditional generation score, since the LUT were not optimized during autoencoding. (2) With full mixup, i.e. $\beta_0 \in [0, 1], \beta_1 \in [0, 1]$, there is a larger variation in the proportion of A_{fg}, B_{fg} to the mixed value $A_{fg_{mix}}$, which turned to be unstable and the reconstruction task suffered.

E. Additional results

E.1. Conditional generation

We supply more conditionally generated images to further demonstrate the conditional generation performance. We use generation conditioned on both very different and very similar classes in order show both the broad coverage and high sensitivity to detail in the various clusters.

In Fig. 7, the images are obtained by generating five different images per each reference image in the top row. To achieve these results, our model has to perform two tasks. First, it has to be able to detect the child and parent classes under which the object is represented. Second, it needs to be able to generate a similar looking object with the predicted classes. The success in this task is evidence for both the generation and clustering capabilities of the model.

In the figure, each column shows a real image, followed by five generated images conditioned on the first image in respect to category. Additionally, in each row, all images are generated with the same z , showing how non-categorical information is consistent across the different categories and how the pose is disentangled from the shape category.

For both birds and dogs, we can see that the generated images have very similar properties to their conditioned image. In both cases, we can see the large coverage of different classes and the fine detailed differences between similar classes. For cars, we can see that that the generated images apply the same color, but the car shape is changing, indicating that the model has categorized the cars by their color and not by their model.

E.2. Reconstruction

We supply more images to show the reconstruction path with the resulting reconstructed images, reconstructed backgrounds, and segmentation masks.

In Fig. 8, the results show the images generated by the reconstruction process. The generated mask shows the model's ability to detect and segment the object, the background image shows the model's ability to repaint the background, and the foreground image shows the model's ability to detect and reconstruct conditioned on the object class.

The segmentation works under many different poses, sizes, and backgrounds. For dogs and cars, it can be seen that our model is sometimes better than the "ground-truth" masks, which were generated by a pre-trained network. The background repainting works well in the majority of cases, but we do notice that some backgrounds work better than others. The challenges are mostly noticeable in the cars dataset, where there was the smallest amount of background patches available in X_{bg} , leading to a less powerful background discriminator. Subsequently, the performance of the background generation was affected.

E.3. Image to image translation

We supply more images, Fig. 9, to show the image to image translation capability of the model. We show that the disentanglement that emerged from the design allows manipulation of the reconstructed image by replacing the child code with a code from an arbitrary category. We can see that not only do the objects in the images change appearance, but the change is consistent across different images, while the background is mostly unaffected.

In birds, we can see that the generator is usually able to detect the different parts of the birds (wings, head, beak) and apply to correct color manipulation to the correct area. Furthermore, the color manipulation works on birds of different shapes and different original colors. The background is sometimes slightly altered, first, because it is regenerated every time, and second, because the foreground mask is soft and sometimes applies a slight manipulation on the background as well. In dogs, the manipulation is less effective, but it is noticeable and is correlated to the applied category. In cars, we can see the color manipulation for many different colors. We can also notice how the background is mostly unchanged and that the manipulation is applied correctly on the car chassis and not on other parts like windows, tires and lights.

E.4. Background inpainting

Due to space limits, we could not address all tasks in the main paper. As an intermediate step of the reconstruction task, our model also performs a side-task of object foreground extraction and background inpainting, see Fig. 4. The model first detects the foreground in the image and produces a segmentation mask. Then, with the mask, the background is encoded and reconstructed. Because the mask is a prediction and not a ground-truth, the model cannot only fill the masked pixels with background texture, but has to assume that the mask was not perfect and reconstruct the entire image. The drawback of this method is that the background is not always identical to the source in the background area, but the benefit is that the object is fully removed even when it is not fully covered by the mask.

We compare our model against images produced with Deep-Image-Prior (DIP; Ulyanov et al., CVPR 2018). There are two variants. In the first, DIP receives the ground-truth mask and in the second, the predicted mask is given. DIP optimizes its network for 1000 steps on the input image.

The results can be seen in Fig. 10. It can be observed that DIP works relatively well when using a perfectly covering mask, but fails when the mask does not fully cover the object. In contrast, our model suffers less when the mask is not perfect. We can also see that our model does not exactly inpaint the background but actually repaints it, which usually results in a slightly different background even where

the image was not masked, but as we mentioned above, it may be beneficial when the mask is not perfect. Finally, our model performs the inpainting task in a single forward path instead of 1000 iterations of DIP.

E.5. User study images

In the main text, we present a user-study to support the conditional generation results, see Tab. 2. We provide the images used in the study in Fig. 11. In the figure, the images are shown order. The participants were shown the images separately and in a random order.

Table 5. The components of the OneGAN model

	Symbol	Description	Computed as (or a comments)
Variables	$\phi_c \in [1, N_C]$	child class	
	$\phi_p \in [1, N_P]$	parent class	
	$\mathbf{e}_c \in \{0, 1\}^{N_C}$	child class one-hot vector (style)	$\mathbf{e}_c[i] = \delta_{i, \phi_c}$
	$\mathbf{e}_p \in \{0, 1\}^{N_P}$	parent class one-hot vector (shape)	$\mathbf{e}_p[i] = \delta_{i, \phi_p}$
	$\mathbf{e}_{bg} \in \{0, 1\}^{N_P}$	background one-hot vector	$\mathbf{e}_{bg} = \mathbf{e}_p$
	$\mathbf{z} \in \mathbb{R}^{d_z}$	pose code	$\mathbf{z}[i] \sim \mathcal{N}(0, 1)$
	$\mathbf{v}_c \in \mathbb{R}^{d_c}$	style code vector	$\mathbf{v}_c = V_{c_0}(\mathbf{e}_c)$
	$\mathbf{v}_p \in \mathbb{R}^{d_p}$	shape code vector	$\mathbf{v}_p = V_{p_0}(\mathbf{e}_p)$
	$\mathbf{v}_{bg} \in \mathbb{R}^{d_{bg}}$	background code vector	$\mathbf{v}_{bg} = V_{bg_0}(\mathbf{e}_{bg})$
	A_{fg}	foreground pre-image	$A_{fg} = G_{fg_0}(\mathbf{v}_p, \mathbf{z})$
	A_{bg}	background pre-image	$A_{bg} = G_{bg_0}(\mathbf{v}_{bg}, \mathbf{z})$
	I_m	foreground mask	
	I_{fg}	foreground image	$(I_{fg}, I_m) = G_{fg_2}(G_{fg_1}(A_{fg}, \mathbf{v}_p), \mathbf{v}_c)$
	I_{bg}	background image	$I_{bg} = G_{bg_1}(A_{bg})$
	I	full image	$I = I_{bg} \circ (1 - I_m) + I_{fg} \circ I_m$
	B_{fg}	foreground bypass	$B_{fg} = E_{p_1}(I)$
	B_{bg}	background bypass	$B_{bg} = E_{bg_1}(I, I_m)$
Networks	X_c	image domain	
	X_{bg}	background image domain	
	V_c	embedding LUT of child class	
	V_p	embedding LUT of parent class	
	V_{bg}	embedding LUT of background	
	G_{fg}	foreground generator, with subnetworks G_{fg_u}	$G_{fg}(\mathbf{v}_c, \mathbf{v}_p, \mathbf{z}) = G_{fg_2}(G_{fg_1}(G_{fg_0}(\mathbf{v}_p, \mathbf{z}), \mathbf{v}_p), \mathbf{v}_c)$
	G_{bg}	background generator, with subnetworks G_{bg_u}	$G_{bg}(\mathbf{v}_{bg}, \mathbf{z}) = G_{bg_1}(G_{bg_0}(\mathbf{v}_{bg}, \mathbf{z}))$
	E_c	style encoder	$E_c(I)$
	E_p	content encoder	$E_p(I)$
	E_{bg}	content encoder	$E_{bg}(I, I_m)$
Parameters	D_c	image discriminator	
	D_{bg}	background discriminator	
	N_C	number of child classes	Depends on the dataset. Sec. 5
	N_P	number of parent classes	$N_P < N_C$, Depends on the dataset.
	d_z	dimensionality of pose code	$d_z = 100$
	d_c	dimensionality of style code	$d_c = 32$
	d_p	dimensionality of shape code	$d_p = 16$
	d_{bg}	dimensionality of background code	$d_{bg} = 32$
	H, W	size of image	$H = W = 128$

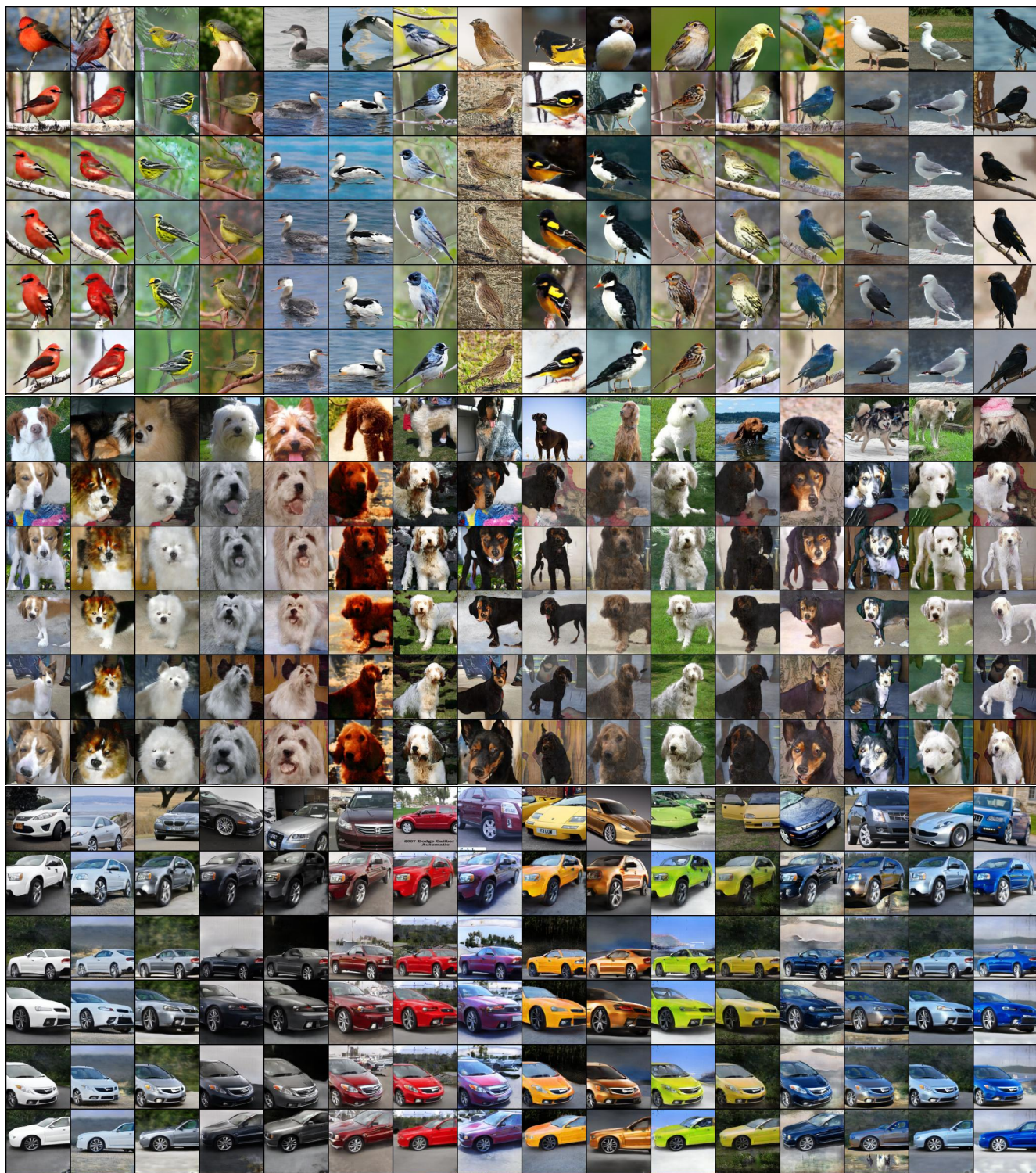


Figure 7. Conditional Image Generation. From top to bottom: (i) real image, (ii-vi) generation of images with the encoded parent and child codes and a different vector z per row.

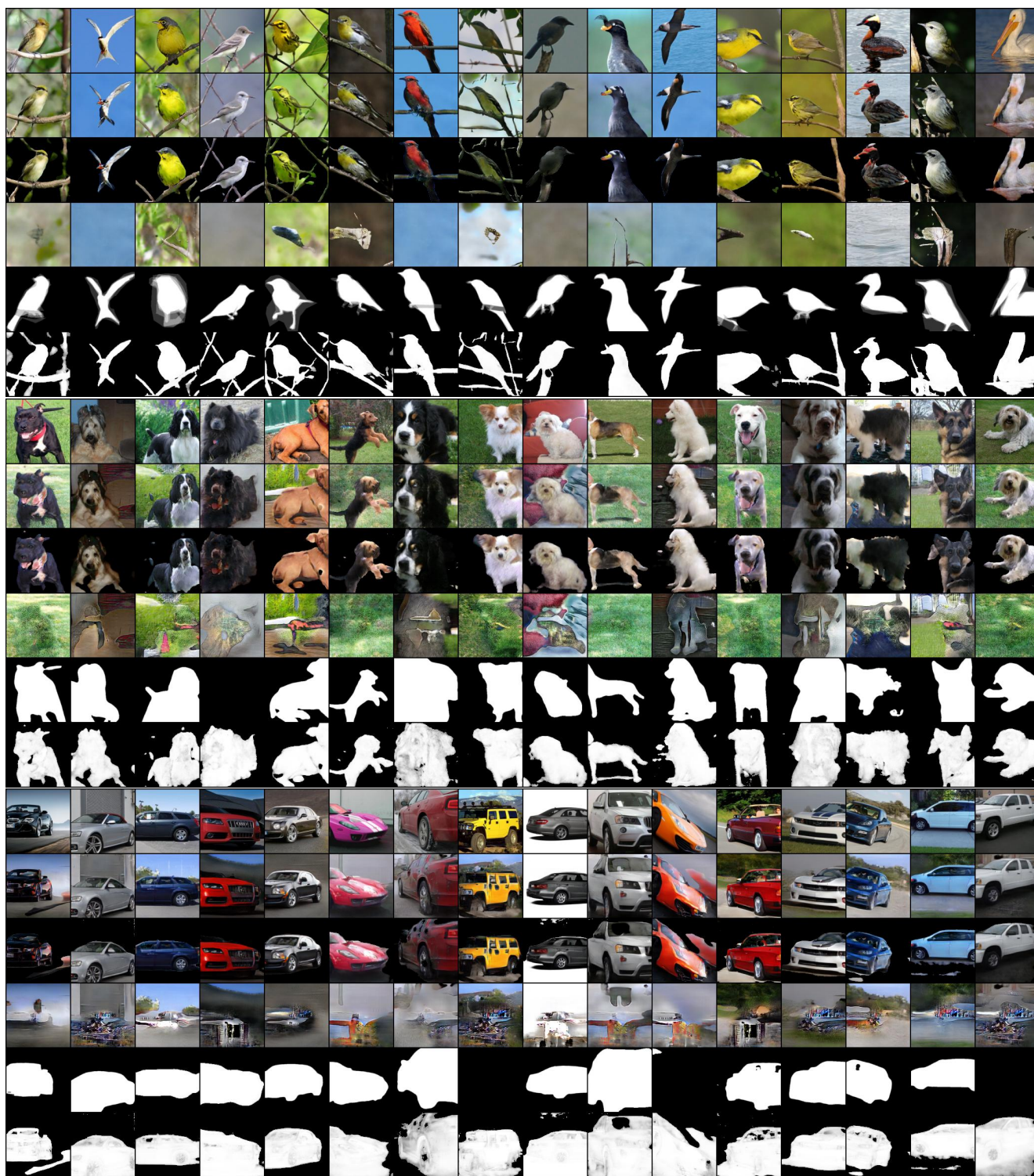


Figure 8. Image Reconstruction. From top to bottom: (i) real image, (ii) reconstructed image, (iii) reconstructed foreground, (iv) reconstructed background, (v) ground-truth foreground mask, (vi) predicted foreground mask.



Figure 9. Image to Image Translation. From left to right: (i) real image, (ii-xiii) reconstructed images when the child code e_c in each column is switched with a code from a selected category represented by the top image.

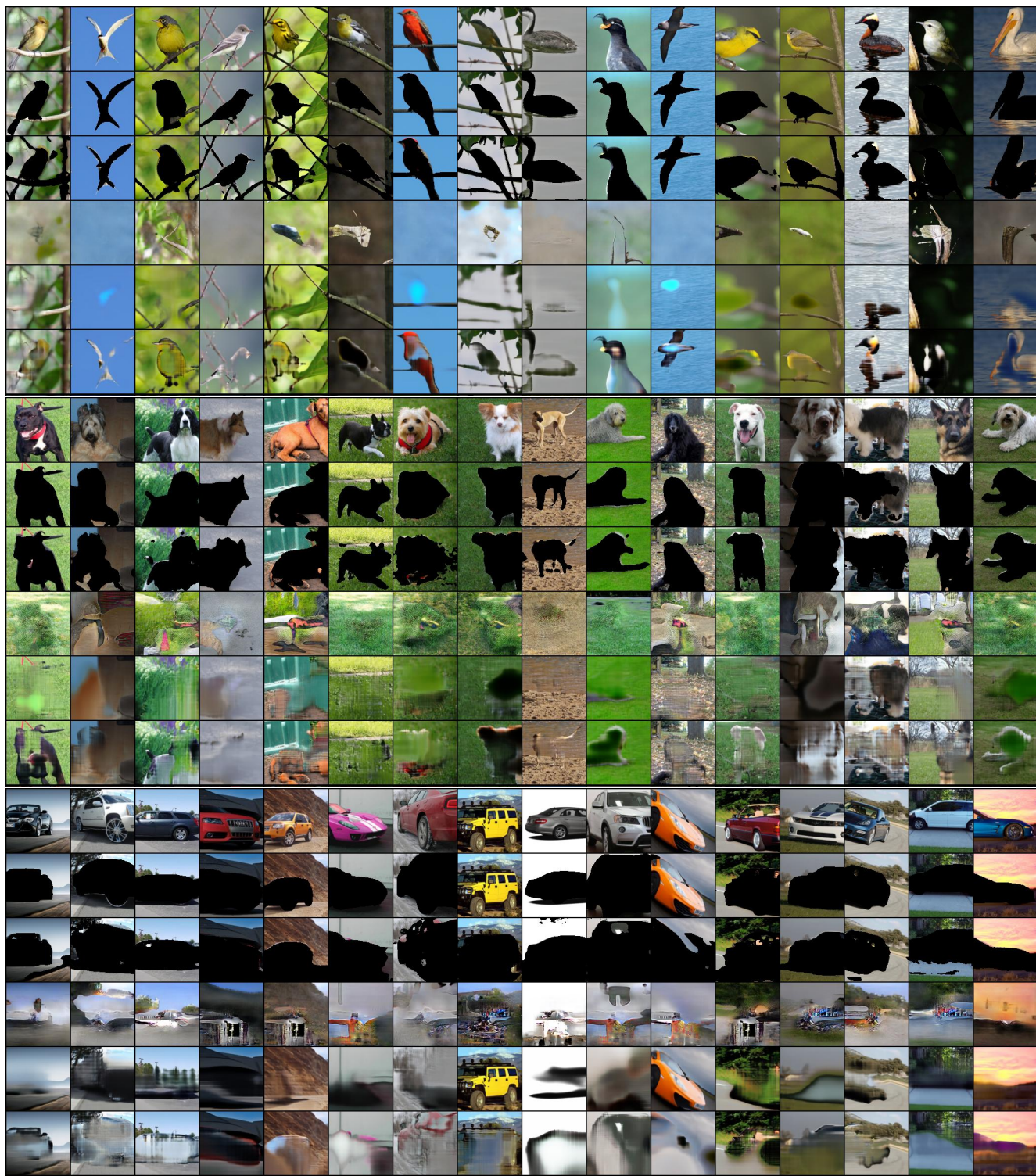


Figure 10. Background Inpainting. From top to bottom: (i) original image, (ii) image masked with real mask, (iii) image masked with predicted mask, (iv) OneGAN, (v) DIP with real mask, (vi) DIP with predicted mask.

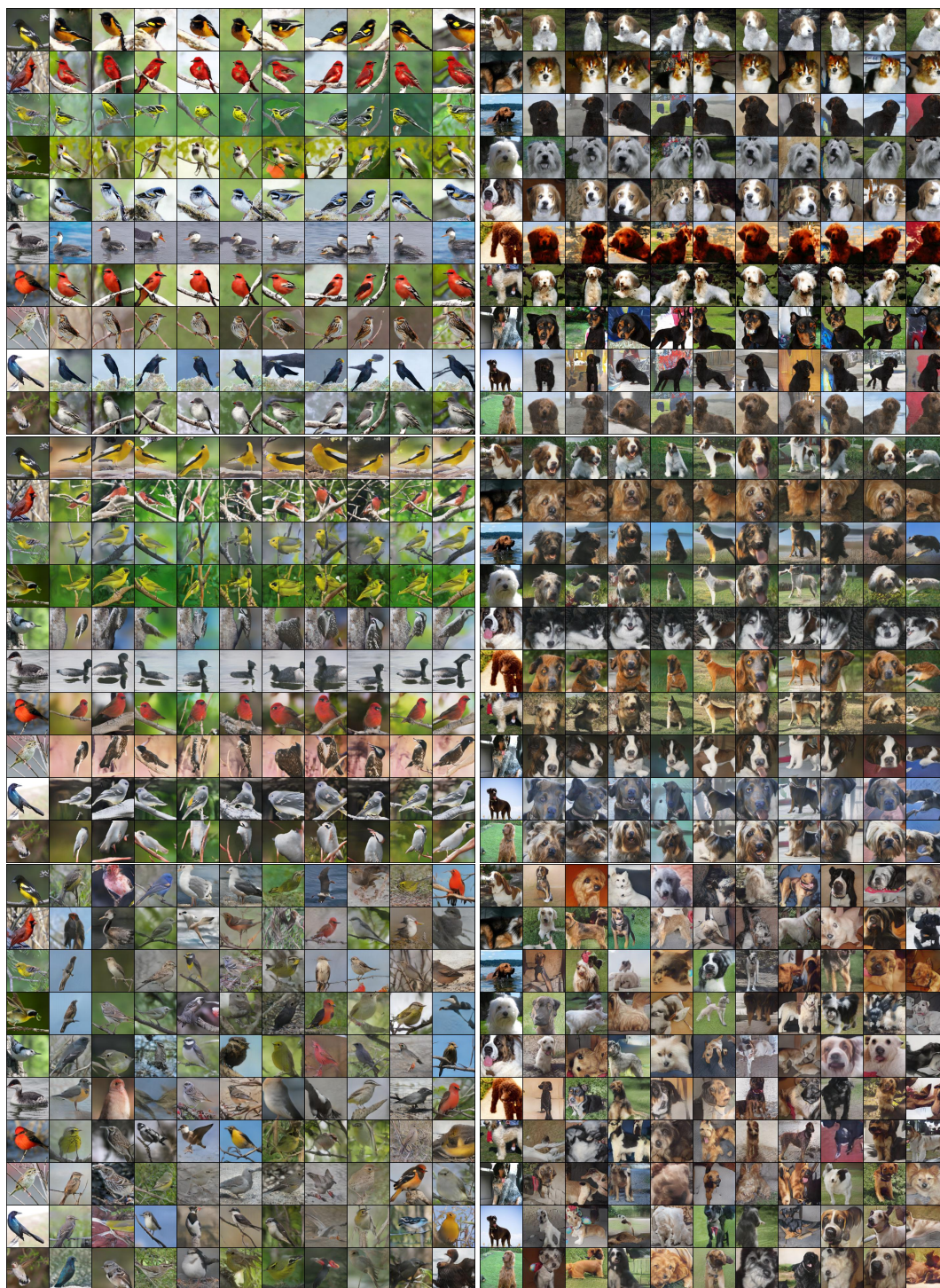


Figure 11. User Study. From top to bottom. (i) OneGAN birds/dogs, (ii) FineGAN birds/dogs, (iii) StackGANv2 birds/dogs. In each row, 10 generated images conditioned upon the real image on the left.

Table 6. General modules

Module	layers	input	output
GLUNorm	ChannelSplit	x	x_L, x_R
	LayerNorm	x_L	x'_L
	Sigmoid	x_R	x'_R
	Multiply	x'_L, x'_R	-
UPBlk (c_i, c_o, S)	Upsample2d($S/2, S$)	-	-
	K3P1Conv2d($c_i, 2c_o$)	-	-
	GLUNorm	-	-
DOWNBlk (c_i, c_o)	K4S2P1Conv2d(c_i, c_o)	-	-
	LayerNorm	-	-
	lReLU(0.2)	-	-
RESBlk0 (c_i)	K3P1Conv2d($c_i, 2c_i$)	x	-
	GLUNorm	-	-
	K3P1Conv2d($c_i, 2c_i$)	-	-
	GLUNorm	-	d
	Add	x, d	-
RESBlk (c_i, d, c_o)	K3P1Conv2d($c_i + d, 2c_i$)	-	-
	GLUNorm	-	-
	RESBlk0(c_i)	-	-
	RESBlk0(c_i)	-	-
	K3P1Conv2d($c_i, 2c_o$)	-	-
	GLUNorm	-	-

Table 7. Background Generator G_{bg}

Module	layers	input	output
V_{bg}	Linear(N_P, d_{bg})	e_{bg}	v_{bg}
G_{bg_0}	Linear($d_{bg} + d_z, 32768$)	v_{bg}, z	-
	Reshape(2048,4,4)	-	-
	GLUNorm	-	-
	UPBlk(1024,512,8)	-	-
G_{bg_1}	UPBlk(512,256,16)	-	A_{bg}
	UPBlk(256,128,32)	A_{bg}	-
	UPBlk(128,64,64)	-	-
	UPBlk(64,32,128)	-	-
	K3P1Conv2d(32,3) + tanh	-	I_{bg}

Table 8. Foreground Generator G_{fg}

Module	layers	input	output
V_p	Linear(N_P, d_p)	e_p	v_p
V_c	Linear(N_C, d_c)	e_c	v_c
G_{fg_0}	Linear($d_p + d_z, 32768$)	v_p, z	-
	Reshape(2048,4,4)	-	-
	GLUNorm	-	-
	UPBlk(1024,512,8)	-	-
G_{fg_1}	UPBlk(512,256,16)	-	A_{fg}
	UPBlk(256,128,32)	A_{fg}	-
	UPBlk(128,64,64)	-	-
	UPBlk(64,3,128)	-	C_{fg_0}
G_{fg_2}	RESBlk(64, d_p , 32)	C_{fg_0}, v_p	C_{fg_1}
	RESBlk(32, d_c , 16)	C_{fg_1}, v_c	C_{fg_2}
	K3P1Conv2d(16,3) + tanh	C_{fg_2}	I_{fg}
	K3P1Conv2d(16,1) + sigmoid	C_{fg_2}	I_m

Table 9. Style Encoder E_c

Module	layers	input	output
E_{c_1}	K4S2P1Conv2d(3, 64)	I	-
	LayerNorm	-	-
	lReLU(0.2)	-	-
	DOWNBlk(64, 128)	-	-
	DOWNBlk(128, 256)	-	H_c
E_{c_0}	DOWNBlk(256, 512)	H_c	-
	DOWNBlk(512, 1048)	-	-
	K3P1Conv2d(1048, 1048)	-	-
	LayerNorm	-	-
	lReLU(0.2)	-	-
	Reshape(16384)	-	-
	Linear(16384, 512)	-	-
	LayerNorm	-	-
	lReLU(0.2)	-	h_c
	Linear(512, N_C)	h_c	\hat{e}_c
	Linear(512, d_c)	h_c	μ_c
	Linear(512, d_c)	h_c	σ_c

Table 10. Shape Encoder E_p

Module	layers	input	output
E_{p_1}	K4S2P1Conv2d(3, 64)	I	-
	LayerNorm	-	-
	lReLU(0.2)	-	-
	DOWNBk(64, 128)	-	-
	DOWNBk(128, 256)	-	H_p
	K3P1Conv2d((256, 512)	H_p	-
E_{p_0}	GLUNorm	-	-
	UPBk(256,256)	-	B_{fg}
	DOWNBk(256, 512)	H_p	-
	DOWNBk(512, 1048)	-	-
	K3P1Conv2d(1048, 1048)	-	-
	LayerNorm	-	-
	lReLU(0.2)	-	-
	Reshape(16384)	-	h
	Linear(16384, 512)	h	-
	LayerNorm	-	-
	lReLU(0.2)	-	h_p
	Linear((512, N_C))	h_p	\hat{e}_p
	Linear(512, d_c)	h_p	μ_p
	Linear(512, d_c)	h_p	σ_p
	Linear(16384, 512)	h	-
	LayerNorm	-	-
	lReLU(0.2)	-	h_z
	Linear(512, d_z)	h_z	μ_z
	Linear(512, d_z)	h_z	σ_z

Table 11. Background Encoder E_{bg}

Module	layers	input	output
E_{bg_1}	K4S2P1Conv2d(4, 64)	I, I_m	-
	DOWNBk(64, 128)	-	-
	DOWNBk(128, 256)	-	H_{bg}
	K3P1Conv2d((256, 512)	H_{bg}	-
	GLUNorm	-	-
	UPBk(256,256)	-	B_{bg}

Table 12. Background Discriminator D_{bg}

Module	layers	input	output
D_{bg}	DonwSample2d(128, 126)	I	-
	K4S2P0Conv2d(3, 64)	-	-
	lReLU(0.2)	-	-
	K4S2P0Conv2d(64, 128)	-	-
	lReLU(0.2)	-	-
	K4S4P0Conv2d(128, 256)	-	-
	lReLU(0.2)	-	$H = D_{bg_C}(I)$
	K4S1P0Conv2d(256,1)	H	$D_{bg_A}(I)$
	K4S1P0Conv2d(256,1)	H	$D_{bg_B}(I)$

Table 13. Object Discriminator D_c

Module	layers	input	output
D_c	K4S2P1Conv2d(4, 64)	I	-
	LayerNorm	-	-
	lReLU(0.2)	-	-
	DOWNBk(64, 128)	-	-
	DOWNBk(128, 256)	-	-
	DOWNBk(256, 512)	-	$D_{cc}(I)$
	DOWNBk(512, 1048)	-	-
	K3P1Conv2d(1048, 1048)	-	-
	LayerNorm	-	-
	lReLU(0.2)	-	-
	Reshape(16384)	-	H
	Linear(16384, 512)	H	-
	LayerNorm	-	-
	lReLU(0.2)	-	-
	Linear(512, 1)	-	$D_{cA}(I)$
	Linear(16384, 512)	H	-
	LayerNorm	-	-
	lReLU(0.2)	-	-
	Linear(16384, 512)	-	$D_{cB}(I)$

Task:	Segmentation	Conditional generation
Metric:	IOU	C-IS
OneGAN	55.5	30.7
no mask-reg	35.3	19.5
no bypass	53.3	22.8
no mixup	54.1	17.5
full mixup	28.8	23.1

Table 14. Additional ablation results on the birds dataset. Comparison is done for segmentation (IOU) and conditional generation (C-IS).